

## Stage-II Recovery in Electron-Irradiated InSb†

F. H. EISEN\*

*Atomics International Division of North American Aviation, Canoga Park, California*

(Received 23 March 1966)

Isochronal and isothermal recovery studies have been carried out in electron-irradiated samples of InSb following irradiation with high-energy electrons, using Hall coefficient and electrical conductivity as measures of the damage. The emphasis in this work has been on the recovery in stage II, and the results show that the recovery depends strongly on the carrier concentration of the sample. The temperature of the center of the recovery stage was observed to vary from 91°K in some *p*-type samples to 203°K in a highly degenerate *n*-type sample. The activation energy for recovery changed from 0.24 to 0.71 eV over this same range of carrier concentrations. These changes have been explained by assuming that the two acceptor levels associated with the radiation-produced defects must be empty in order for annihilation of the defects to occur. The details of the analysis relating these recovery parameters to the sample carrier concentration are presented. In order to fit the observed recovery kinetics, it is assumed that two close interstitial-vacancy pairs produced by the irradiation are involved, and that they annihilate by basically first-order processes with different rate constants. A model for the defects and their mode of annihilation, assuming vacancies to be the mobile species, is suggested.

### I. INTRODUCTION

INDIUM antimonide is the most extensively investigated III-V compound with regard to radiation-damage studies. The first studies of damage recovery following electron irradiation were reported by Aukerman.<sup>1</sup> Vook<sup>2</sup> has measured changes in sample length and thermal conductivity following electron irradiation and during annealing. Georgopoulos *et al.*<sup>3</sup> have reported work using neutron and gamma irradiation. The present author has previously reported the results of electron-radiation-damage studies in several *n*-type samples of InSb.<sup>4</sup> This work has been extended to *p*-type samples and to *n*-type samples with initial electron concentrations higher and lower than the range of concentrations in the previous work. The results show that the recovery process in InSb following electron irradiation is strongly dependent on the carrier concentration of the sample. For example, the temperatures at which the first four recovery stages occur generally become lower as the Fermi level is lowered upon using samples of lower electron concentration. In the present report we concentrate on the second recovery stage, which was also treated in the greatest detail in the previous work. Data are presented showing a variation of the recovery temperature from 91 to 203°K and of the apparent activation energy for recovery from 0.24 to 0.71 eV, as well as changes in the apparent recovery kinetics. A detailed treatment of the variation

of these parameters as a function of the carrier concentration of the sample is presented, based on the assumption that the two acceptor levels associated with the defects must be empty for defect annihilation to occur. Finally, a model is suggested for the structure of the defects and their mode of production and annihilation, based on the present work and upon orientation-dependent experiments reported previously.<sup>5</sup>

### II. EXPERIMENTAL TECHNIQUE

The experimental methods were generally similar to those described previously.<sup>4</sup> The samples were about 0.005 in. thick and were usually cut from wafers of this thickness, polished to a Linde "B" finish, which were purchased from Cominco Products, Spokane, Washington. Electrical contacts were applied to the *p*-type samples by alloying indium to the sample arms during a 15-min 200°C anneal in vacuum and using indium solder to secure leads to the indium on the arms.

Most irradiations were carried out at liquid-nitrogen temperature using a cryostat similar to that described previously.<sup>4</sup> In *p*-type samples where stage-II recovery occurs near liquid-nitrogen temperature, some irradiations were also carried out at liquid-helium temperature. The helium cryostat was basically similar in design to the nitrogen cryostat and has been described in detail elsewhere.<sup>6</sup> In both these cryostats the manganin wire heaters have been replaced by a heater element consisting of a pair of 0.005-in. Nichrome wires packed in MgO insulation inside a stainless-steel sheath which is silver soldered to the copper piece on which the manganin wire was formerly wound. The connection of leads to the sample has been simplified by the addition of a sapphire tie point to the sample mounting plate, providing a support for the leads near the sample.

† Present address: North American Aviation Science Center, Thousand Oaks, California.

\* Based on work sponsored by the Metallurgy Branch, Division of Research, U. S. Atomic Energy Commission, under Contract No. AT-(11-1)-GEN-8.

<sup>1</sup> L. W. Aukerman, *Phys. Rev.* **115**, 1125 (1959).

<sup>2</sup> F. L. Vook, *J. Phys. Soc. Japan* **18**, Suppl. 2, 190 (1963); *Phys. Rev.* **135**, A1750 (1964).

<sup>3</sup> C. Georgopoulos, M. Verdone, and D. Dautreppe, *Compt. Rend.* **257**, 2640 (1963). M. Verdone, C. Georgopoulos, and D. Dautreppe, in *Radiation Damage in Semiconductors* (Dunod Cie., Paris, 1965), p. 205.

<sup>4</sup> F. H. Eisen, *Phys. Rev.* **123**, 736 (1961).

<sup>5</sup> F. H. Eisen, *Phys. Rev.* **135**, A1394 (1964).

<sup>6</sup> F. H. Eisen, in *Advances in Cryogenic Engineering* (Plenum Press, Inc., New York, 1963), Vol. 8, p. 437.

Because of the high thermal conductivity of the sapphire, the use of this tie point also helps decrease thermal gradients in the sample due to the conduction of heat to or from the sample through the electrical leads fastened to the sample.

### III. RESULTS AND DISCUSSION

#### A. General Features of the Irradiation Experiments

The recovery data presented were obtained following irradiation with 1.0-MeV electrons (with one specific exception noted below) at or below liquid-nitrogen temperature. Measurements of the Hall coefficient and electrical conductivity were used to determine the changes in carrier concentration and mobility produced by the irradiation and subsequent annealing. The 1.0-MeV electron irradiation produced a decrease in electron concentration at liquid-nitrogen temperature in all the samples studied, i.e., *n*-type samples became less *n*-type and *p*-type samples became more *p*-type.<sup>7</sup> The recovery during stage-II annealing was always in the direction of increasing electron concentration.

Both isochronal and isothermal annealing experiments were carried out. The carrier concentration usually varied linearly with the integrated beam current during the irradiations so that the defect concentration could be assumed to be linearly related to the change in carrier concentration during the annealing experiments. In this case, the fraction of defects not yet annihilated in a particular recovery stage  $\varphi$  may be taken as the ratio of the carrier concentration not recovered in that stage to the total carrier-concentration recovery in the stage. In those cases where the Fermi level was near a defect energy level, the above-mentioned linear relation did not hold and the exposure curve was used to correct the isothermal carrier-concentration recovery data so that  $\varphi$  was obtained. This was accomplished by assuming that the number of defects depends linearly on the integrated beam current so that the relation between change in carrier concentration and number of defects is the same as that between change in carrier concentration and integrated beam current.

The data consist mainly of isochronal (heating rate about 1.5°/min) and isothermal recovery measurements on a variety of *n*- and *p*-type samples of InSb. Figure 1 shows a typical isochronal recovery curve for an *n*-type sample (*N7*,  $n_0 = 1.5 \times 10^{16} \text{ cm}^{-3}$ ). The only significant difference in *n*-type samples with lower values of  $n_0$  is that the recovery temperatures for stages I through IV are observed to decrease as  $n_0$  decreases. Also

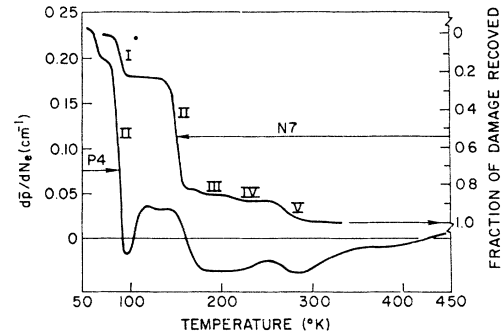


FIG. 1. Isochronal recovery curve for an *n*-type sample (*N7*,  $n_0 = 1.5 \times 10^{16} \text{ cm}^{-3}$ ) and a *p*-type sample (*P4*,  $p_0 = 1.4 \times 10^{16} \text{ cm}^{-3}$ ) of InSb following irradiation with 1.0-MeV electrons at 78°K. For clarity, the experimental points are omitted.

shown in Fig. 1 is the isochronal recovery curve for a *p*-type sample (*P4*,  $p_0 = 1.4 \times 10^{16} \text{ cm}^{-3}$ ). The most noticeable difference between the *n*-type and *p*-type samples is the appearance of several reversals in direction of the carrier-concentration change during annealing in the *p*-type sample.

#### B. Identification of Stages in *p*-Type Samples

Because of the differences in the isochronal recovery curves for *p*- and *n*-type samples, it is not immediately clear which regions of recovery in *p*-type samples correspond to the stages which were first observed in recovery studies in *n*-type samples. A point of primary interest in the present work is the identification of stage II in *p*-type samples. The identification is facilitated by the fact that stage II has the lowest threshold displacement energy.<sup>4,5</sup> Thus, it is possible by irradiating at low enough electron energy (400 eV) to produce only damage which recovers in stage II. The results of such low-energy irradiations of *p*-type samples indicate that stage II is the one so labeled on the curve for sample *P4* of Fig. 1. It is probable that the stage below stage II on the curve for *P4* is stage I, and it has been possible to identify stages III, IV, and V in *p*-type samples from the dependence of their recovery temperature on carrier concentration.<sup>8</sup> A detailed description of this work, as well as other features of these recovery stages, will be reserved for a subsequent publication.

#### C. Stage II

##### 1. Experimental Variation of Recovery Parameters with Carrier Concentration

The dependence of the temperature  $T_c$  at the center of stage II (taken as the temperature at which half of the recovery has occurred) on carrier concentration in *n*- and *p*-type samples is shown in Fig. 2. It is seen that there is a variation of the observed values of  $T_c$  from

<sup>7</sup> This is in contrast with the results of Aukerman in Ref. 1 who finds that there is a final Fermi level about 0.03 eV above the valence band when irradiating at 78°K with 4.5-MeV electrons. There seems to be a donor level associated with the defects which annihilate in stage V and since a greater fraction of the damage recovers in this stage following the higher energy irradiation, a movement of the position of the final Fermi level to a point farther above the valence-band edge seems reasonable.

<sup>8</sup> F. H. Eisen, Bull. Am. Phys. Soc. 10, 360 (1965).

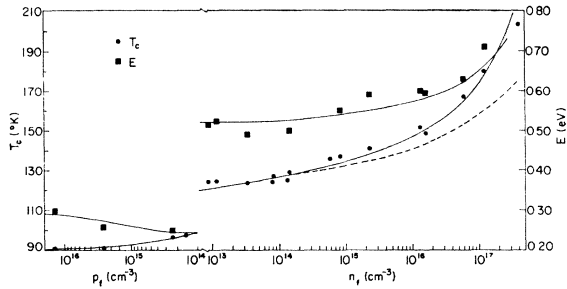


FIG. 2. Recovery temperature  $T_c$  and activation energy for recovery  $E$  as a function of the carrier concentration following state-II recovery. The solid and dashed lines were calculated by a procedure described in the text.

91 to 203°K over the range of carrier concentrations for which measurements were made.

The isochronal recovery data can be combined with isothermal measurements to calculate  $E$ , the activation energy for recovery, by method of Meechan and Brinkman<sup>9</sup> as described in Ref. 4. The results of this calculation are also shown in Fig. 2 for most of the samples for which a value of  $T_c$  was measured. The measured values of  $E$  range from 0.25 to 0.71 eV. The curves drawn in Fig. 2 are the values of  $T_c$  and  $E$  calculated from a model which is described below.

The observed recovery kinetics were also found to depend on the sample carrier concentration over the whole range of concentrations for which measurements were carried out. The change was such that the relative time duration of the isothermal recovery was greater in samples of higher electron concentration.

## 2. Energy Levels of the Stage-II Defects

Figure 3 shows initial values of the carrier removal rate for stage II in various samples, plotted as a function of the position of the Fermi level in the sample. Such a plot can be used to determine the position of the defect energy levels since it can be shown that the carrier removal rate should change rather abruptly when the Fermi level is near a defect level and should be relatively constant when the Fermi level is several units of  $kT$  away from a defect level.<sup>10</sup> An inspection of Fig. 3 indicates that there are two energy levels associated with the defects that annihilate in stage II, one about 0.04 eV above the valence band (level 1) and the other about 0.03 eV below the conduction band (level 2).<sup>11</sup> The fact that  $-d\bar{n}/dN_e + d\bar{p}/dN_e$  is always

<sup>9</sup> C. J. Meechan and J. A. Brinkman, Phys. Rev. **103**, 1193 (1956).

<sup>10</sup> H. Y. Fan and K. Lark-Horowitz, in *Effects of Radiation on Materials*, edited by J. J. Harwood, H. H. Hausner, J. Morse, and W. Rauch (Reinhold Publishing Corporation, New York, 1958), p. 166.

<sup>11</sup> Measurements of the Hall coefficient versus temperature in both  $n$ -type and  $p$ -type samples give no indication of the presence of any chemical impurity levels near either of these levels so that the conclusion that they are due to defects produced by the electron irradiation is justified.

positive, as indicated in Fig. 3, implies that both levels are acceptor levels. If both acceptor and donor levels were present, the stage-II defects should exhibit donor behavior in some samples. Since the stage-II defects acted as acceptors in samples with the Fermi level ranging from 0.02 eV above the valence band to well into the conduction band, it can be concluded that both level 1 and level 2 are acceptor levels.

## 3. Qualitative Description of the Model for the Carrier Concentration Dependence of the Recovery

It is assumed that the defect-annihilation rate is proportional to the number of defects for which level 1 is empty. If the Fermi level is several units of  $kT$  below level 1, this will be essentially all the defects, but as the Fermi level rises higher in the band gap the defect-annihilation rate at a given temperature will decrease because of the decreasing degree of ionization of level 1. This results in  $T_c$  increasing in samples of increasingly higher electron concentration as shown in Fig. 2. The measured activation energy for recovery will include a contribution from the energy necessary to remove electrons from level 1. It can be seen that there will be a substantial difference in  $E$  between  $p$ -type and  $n$ -type samples, as observed, because in  $p$ -type samples the electron moves to a lower energy state when level 1 becomes ionized, whereas in  $n$ -type samples the electron must be excited from level 1 to the conduction band. The equations for the rate of annihilation of the defects contain a temperature-dependent factor outside the Boltzmann factor. This leads to additional changes in the apparent activation energy which is obtained when the total temperature dependence of the annihilation rate is represented in the Boltzmann form.

The above assumption also results in a dependence of the observed recovery kinetics on the sample carrier concentration. If the Fermi level is several units of  $kT$  below level 1, the kinetics should be first order since

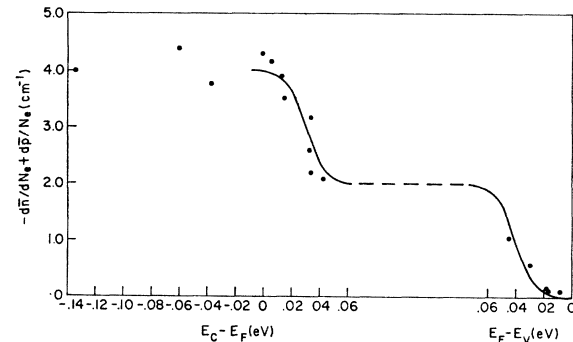


FIG. 3. Initial values of the carrier removal rate in stage II for irradiation with 1.0-MeV electrons as a function of the Fermi level in the sample. The solid curves show the form of the Fermi-Dirac function at 78°K assuming the generation rate for both levels is  $2.0 \text{ cm}^{-1}$ , that the upper level is at 0.03 eV below the conduction band, and that the lower level is 0.04 eV above the valence band.

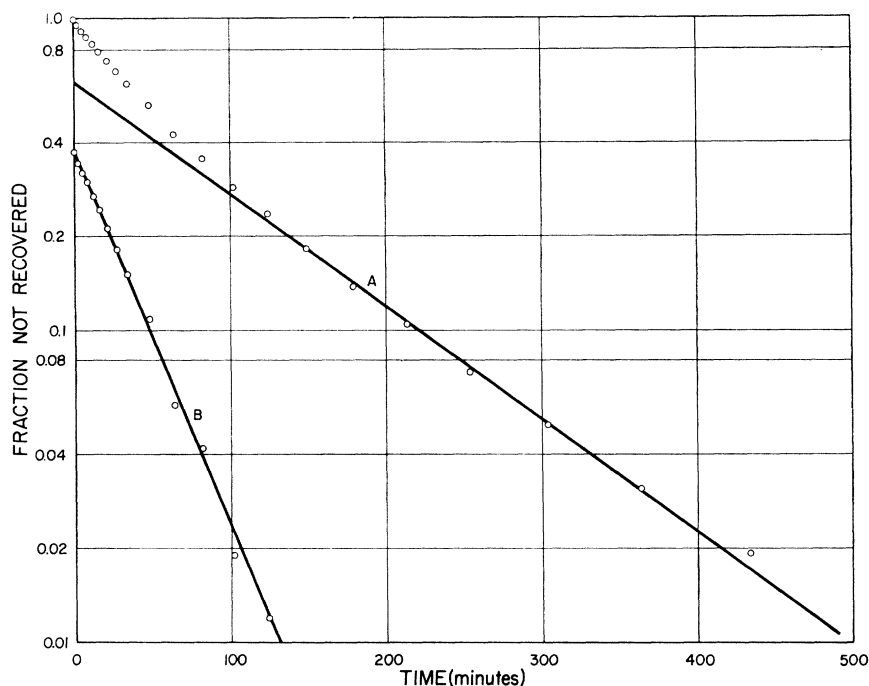


FIG. 4. Stage-II isothermal data for sample *P4*. The upper set of points represent the experimental data. The lower set of points was obtained by subtracting the extrapolation of the upper exponential to short times from the experimental points.

nearly all the defects are in the proper charge state for annihilation. As the Fermi level rises higher this is no longer the case, and the fraction of the defects which are in the proper charge state for annihilation changes due to the small shift in the Fermi-level position as the recovery proceeds. The result is a deviation of the kinetics from first order. Actually, it is necessary to assume that the recovery proceeds by two first-order processes perturbed in the above manner. This was also done in Ref. 4, but in the present case there is direct experimental evidence to support this assumption. Figure 4 shows a plot of a  $\log \varphi$  versus time for sample *P4* in which the Fermi level, was about 0.02 eV below level 1 so that there should be no perturbation of the postulated first-order decays. In samples with the Fermi level somewhat above level 1, the kinetics is observed to deviate from that of sample *P4*, lending qualitative support to the assumption that level 1 must be empty for the annihilation of defects to proceed.

In *n*-type samples with high enough electron concentration, level 2 will become occupied and the effect of its degree of ionization on the rate of recovery must also be considered. It is shown below that this level must also be considered. It is shown below that this level must also be empty for the annihilation of defects to proceed. This results in a higher rate of increase of  $T_c$  and  $E$  with increasing electron concentration and further deviations of the observed kinetics from the sum of two exponentials.

This treatment of the dependence of the recovery parameters on carrier concentration gives no information on the mechanism by which the defect annihila-

tion is influenced by the charge state of the defects. Since the recovery proceeds when the levels are empty, i.e., when the acceptor has a more positive charge, it does not seem as though the effect can be due to a repulsion or attraction between the interstitial and the vacancy. Assuming that the vacancy acts as the acceptor, for such an interaction to make the annihilation of the interstitial-vacancy pair more probable when the vacancy changes to a more positive charge would require the unlikely circumstances that the charge on the interstitial be negative whether the effect was due to the removal of a repulsion or the production of an attractive force.

#### 4. Calculation of $T_c$ and $E$

The detailed derivation of the effects on a single first-order recovery stage of the requirement that level 1 be empty for defect annihilation to occur is contained in the Appendix. At this point the application of these results to stage II is discussed, beginning with the calculation of  $T_c$  as a function of the carrier concentration of the sample.

The equations derived for  $T_c$  are the result of calculating the temperature at which half the recovery in a first-order stage would have occurred during isochronal annealing in terms of  $T_{c0}$ , the corresponding temperature in samples with  $p_0$  sufficiently high so that  $T_c$  is independent of  $p_0$ . The carrier-concentration dependence of the temperature at which any other reference value of  $\varphi$  occurs on the isochronal recovery curve can be calculated from the same formulas with

TABLE I. Constants used in calculating  $T_c$  and  $E$ .

$E_{g0}$	0.25 eV
$E_{a1}$	-0.04 eV
$E_{a2}$	0.03 eV
$T_{c0}$	90.3°K
$E_m$	0.295 eV
$\beta$	$2.9 \times 10^{-4} \text{ eV/}^\circ\text{K}$
$N_v$	$3.36 \times 10^{14} T^{3/2} \text{ cm}^{-3}$
$N_c$	$8.87 \times 10^{12} T^{3/2} \text{ cm}^{-3}$
$\lambda_1, \lambda_2$	1.0

the substitution of the appropriate temperature for  $T_{c0}$ . Since stage II actually consists of two first-order substages with slightly different rate constants, the center of the total stage will not be located at the center of either of the substages. However, if the ratio of the rate constants for the two substages is independent of carrier concentration, the fractional recovery in each of the substages at the center of stage II will be the same in all samples. It is shown below that this requirement on the ratio of the rate constants is approximately obeyed. The calculation of the temperature at the center of stage II is therefore equivalent to the calculation of the temperature at some fixed reference value of  $\varphi$  on the isochronal recovery curve for one of the substages with  $T_{c0}$  the temperature at this point in samples with high hole concentrations. The use of the formulas for  $T_c$  derived in the Appendix is therefore justified. The application of the formulas for  $E$  to stage II is likewise justified if the above requirement for the ratio of the rate constants holds since this implies equal values of  $E$  for the two substages.

The values of various parameters used in the calculation of  $T_c$  and  $E$  versus sample carrier concentration are listed in Table I. The values of  $E_{a1}$  and  $E_{a2}$ , the positions of the lower and upper acceptor levels measured, respectively, from the valence-band edge and conduction-band edge, were taken as the energies at the midpoints of the steps in Fig. 3. This is consistent with the assumption that  $\lambda_1$  and  $\lambda_2$ , the statistical-weight ratios for the two levels, are equal to unity. The use of these values for  $\lambda_1$  and  $\lambda_2$  should not cause appreciable error in the calculated values of  $T_c$  and  $E$ . The values of  $T_{c0}$  and  $E_m$  were chosen by adjusting them to give the best fit of the curves for  $p$ -type material to the experimental points. No other adjustments of the parameters used in the calculation of  $T_c$  and  $E$  were made.

The agreement of the calculated curves for  $T_c$  and  $E$  shown in Fig. 2 with the experimental points is quite satisfactory. The dashed curve for  $T_c$  was calculated assuming that it is not necessary for level 2 to be empty for defect annihilation to occur, whereas the solid curve is based on the assumption that level 2 must be empty. The agreement of the experimental points with the solid curve indicates that the latter assumption is correct. It is particularly interesting to note that the decline of  $E$  while  $T_c$  is increasing in  $p$ -type

samples is correctly predicted. The physical basis for this and the large increase in  $E$  in going to  $n$ -type samples is that in the  $p$ -type samples with Fermi level above level 1, the electrons go to a state of lower energy (the valence band) when they vacate level 1, whereas in  $n$ -type samples they must be raised to the conduction band, a state of higher energy. It is also worth noting that the percentage variation in  $E$  is somewhat greater than that in  $T_c$ . The over-all agreement of the computed curve with the data, particularly in light of the above points, is substantial support for the correctness of the model for the carrier-concentration dependence of the recovery parameters. Several of the  $n$ -type samples with low electron ( $< 10^{14} \text{ cm}^{-3}$ ) concentrations were compensated, so that their total impurity concentration was greater than  $10^{16} \text{ cm}^{-3}$ . The values of  $T_c$  and  $E$  are in agreement with the above model, indicating that they are indeed controlled by the carrier concentration and not by the impurity concentration of the sample.

#### 5. Calculation of the Observed Recovery Kinetics

It is also of interest to compare the isothermal-recovery data with the predicted form for the kinetics contained in the Appendix. It is again necessary to take into account the fact that stage II consists of two nearly first-order substages; i.e., to assume

$$\varphi = \alpha \varphi_1 + (1 - \alpha) \varphi_2,$$

where  $\varphi_1$  and  $\varphi_2$  represent the fraction of damage remaining in the two substages.

The value of  $\alpha$  is taken at 0.365 using the data of Fig. 4 (sample P4) for which the  $\varphi_i$  are simple exponential functions of the time. In samples with the Fermi level farther above the valence band than for P4, the rate equation involves the instantaneous carrier concentration and, therefore, the equations for the two substages are coupled through the dependence of this carrier concentration on both  $\varphi_1$  and  $\varphi_2$ . To simplify the calculation of  $\varphi_1$  and  $\varphi_2$ , the approximation is made that the recovery in substage 1 is complete before significant recovery has occurred in substage 2. The dependence of  $\varphi_1$  and  $\varphi_2$  on time can then be determined from the appropriate relation of the form

$$f(\varphi_i) = -K_i t,$$

contained in the Appendix. Equation (5) applies to  $p$ -type samples, Eq. (15) or (22) to nondegenerate  $n$ -type samples, and the result for degenerate  $n$ -type samples may be obtained by numerical integration of Eq. (24).

In addition to determining  $\varphi_i$  versus  $K_i t$  from the appropriate one of these equations, it is also necessary to know the value of  $K_1/K_2$  in order to calculate  $\varphi$  versus  $t$ . The value of  $K_1/K_2$  in different carrier-concentration regions as determined from the above-mentioned equations is given in Table II. Since  $T_c$  is a

TABLE II. Values of  $K_1/K_2$  at various carrier concentrations.<sup>a</sup>

Type	Carrier concentration (cm <sup>-3</sup> )	$K_1/K_2$
$p$	$\lesssim 3 \times 10^{14}$	$(\nu_1/\nu_2)\exp[(E_{m2}-E_{m1})/kT]$
$n$	$\lesssim 3 \times 10^{14}$	$(\nu_1/\nu_2)\exp[(E_{m2}-E_{m1}+E_{a11}-E_{a12})/kT]$
$n$	$\gtrsim 10^{16}$	$(\nu_1/\nu_2)\exp[(E_{m2}-E_{m1}+E_{a11}-E_{a12}-E_{a21}+E_{a22})/kT]$

<sup>a</sup> The final subscript on each quantity denotes the substage to which that quantity applies.

function of carrier concentration,  $K_1/K_2$  will depend on carrier concentration if the argument of any of the exponentials in Table II is different from zero. The procedure which was followed in fitting the calculated kinetics to the isothermal recovery data was to treat  $K_1/K_2$  as a parameter which was adjusted to obtain the best fit. The result of applying this procedure to the data for several  $n$ -type samples is shown in Fig. 5.

The fit of the calculated curves to the isothermal data is not highly sensitive to the value of  $K_1/K_2$  so that  $K_1/K_2$  could not be determined very accurately for a given sample. The values range from 3.25 for sample *P4* to 3.8 for sample *N7*. When  $\ln(K_1/K_2)$  is plotted versus  $1/T$ , the result is approximately a straight line which can be represented by an activation energy of 0.03 eV and a value of  $K_1/K_2=4.6$  at  $1/T=0$ . There are not enough data available for samples in any one of the carrier-concentration regions of Table II to permit the determination of the arguments of any one of the exponential expressions in the table. A consideration of the possible relative values of  $E_m$ ,  $E_{a1}$ , and  $E_{a2}$  for the two substages indicates that in order to obtain the observed increase in the value of  $K_1/K_2$  in going from  $p$ -type to  $n$ -type samples, the relation  $E_{m2} \leq E_{m1}$  must hold. It is probable that  $E_{m1}-E_{m2} \leq 0.006$  eV with 0.003 eV the most likely value.

The calculated curve for sample *N7* in Fig. 5 shows some deviation from the experimental points at both ends. The data shown for sample *N29* exhibit a better fit to the curve calculated for that sample, but the value of  $\Delta n/n_f$  for this data was less than that for *N7* ( $\Delta n$ =the total change in carrier concentration during stage-II recovery,  $n_f$ =the carrier concentration after stage-II recovery is completed). Data from an irradiation of *N29* for which  $\Delta n/n_f$  was comparable with that for *N7* reveal a similar but somewhat smaller tendency to deviate from the calculated curve. These deviations have not been investigated in detail. They are not large enough to be important in calculating the dependence of  $T_c$  and  $E$  on carrier concentration. They may result from a gradual failure with increasing carrier concentration of the approximation of separating the two substages in calculating the expected form of the isothermal recovery curve. Such an effect would increase as  $\Delta n/n_f$  increases since the coupling of the dif-

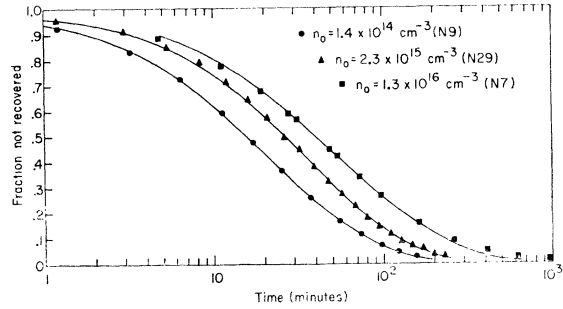


FIG. 5. Stage-II isothermal recovery data for three  $n$ -type samples. The curves were calculated as described in the text. The time scale for two of the samples has been changed by the following factors for convenience in displaying the data: *N9*, 0.38; *N29*, 0.60. Sample *N7* was irradiated at 0.7 MeV; these other two were irradiated at 1.0 MeV. The annealing temperatures were: *N9*, 124°K; *N29*, 135°K; *N7*, 145°K.

ferential equations for  $\varphi_1$  and  $\varphi_2$  disappears as  $\Delta n/n_f$  approaches zero.

### 6. Defect Model

It is assumed that the defects which annihilate in stage II are primary interstitial-vacancy pairs. Many of the experimental observations supporting this assumption have been presented and discussed in Ref. 4. These include the recovery of the Hall coefficient and electrical conductivity to pre-irradiation values following low-energy irradiations in which only damage that anneals out in stage II is produced. Further evidence includes the low threshold energy and the observation of the same damage rate in liquid-nitrogen-temperature and liquid-helium-temperature irradiation of  $n$ -type samples, with no recovery before the temperature region of stages I and II. The present work has included the irradiation of several samples of low electron concentration which were heavily compensated. The recovery occurred in the temperature region which is predicted from the model for the carrier-concentration dependence of the recovery as mentioned above. Also, the damage rates in these samples are in agreement with that in other samples of similar carrier concentration which were not compensated. This independence of the total carrier concentration is further indication that interaction of the primary-radiation-induced defects with impurities has not occurred in the temperature region of stage II.

It is possible to explain the observation of two exponential decays in the isothermal recovery data by assuming that two different defect configurations, which have slightly different decay constants, are produced by the irradiation. This assumption has been implicitly made in the discussion above. However, it is also possible to obtain two exponential decays if there is a single defect pair configuration but two different paths for the defect to follow during the annihilation process. It seems unlikely that this is the correct approach since

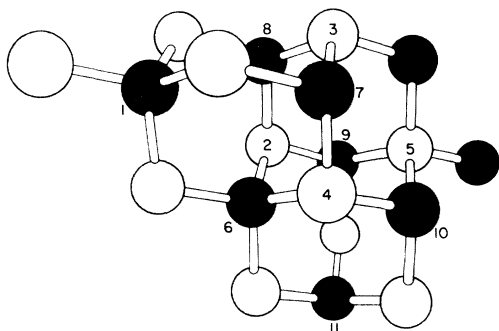


FIG. 6. A portion of a model of the crystal structure of InSb. The numbers label atom positions referred to in the text.

the energies of motion along the two paths would probably not be as close together as the discussion in the preceding section indicated they should be. Also, in the analysis of any such process, it is found that the relative amounts of the recovery occurring in each of the exponential decays would be a function of the relative rate constants for the individual jumps in the annihilation process. This would lead to a temperature dependence of  $\alpha$ , which is not observed. If there are indeed two different interstitial-vacancy pair configurations, it should be possible to observe separate threshold displacement energies for the production of each configuration. Preliminary results of experiments in which isothermal recovery measurements were made as a function of the bombarding electron energy near threshold indicate that such separate thresholds do exist. The data are difficult to analyze because near threshold a thin region of damage is produced in the sample. In this region the carrier-concentration change is sufficient to produce changes in the apparent recovery kinetics similar to those expected from changes in the relative number of the two pair configurations.

The two pair configurations might be formed either by the displacement of one type of atom to two different interstitial positions or through one configuration being formed by the displacement of indium atoms and the other by the displacement of antimony atoms. Previous work<sup>5</sup> indicates that the damage which recovers in stage II is entirely due to the displacement of indium atoms. Therefore, only the first possibility mentioned above need be considered.

In order to pursue the possibility of two pair configurations, we consider how they might be produced in the displacement process. A portion of a model of the crystal structure of InSb is shown in Fig. 6. Consider the displacement of "atom 1." Other work<sup>5</sup> has indicated that this probably occurs along a (111) direction which is along the line joining "atom 1" with "atom 5" in Fig. 6. The motion of atom 1 along this direction is limited by atom 5, and it is likely that the interstitial position surrounded by atoms 2, 3, 4, and 5 is the first stable position along this direction. This position will

be referred to as an "a position," and the defect pair formed by the displacement of atom 1 to this position will be called an "a pair". If atom 1 is directed slightly off the (111) direction during the displacement process, then it may pass through the barrier formed by atoms 2, 4, 5, 6, 9, and 10 into a position surrounded by atoms 6, 9, 10, and 11, rather than stop in the a position. This position will be called a "b position" and the defect pair a "b pair."

Consider now the possible modes of annihilation of a and b pairs. If the interstitial is the mobile defect, then the interstitial in the b position must move first into the a position during the process of annihilation. An analysis of the kinetics of recovery of the sum of the a pairs and b pairs reveals the same situation as for two recovery paths of a single defect; i.e., the value of  $\alpha$  would be expected to be temperature-dependent. Since no temperature dependence is observed, we are led to consider the possibility that the vacancy is the mobile defect. For an a pair, atom positions 6, 7, and 8 are equivalent positions to which the vacancy can jump from position 1. The annihilation of an interstitial in an a position with a vacancy on one of these three is likely to proceed at a much faster rate than the original jump of the vacancy so that this first jump is the rate-limiting step in the annihilation process. For the b pair, only the jump to atom position 6 would place the vacancy in a position where rapid annihilation of the interstitial-vacancy pair would be expected. This jump of the vacancy to a position near a b pair should proceed at about the same rate as the jump of the vacancy of an a pair to one of the above-enumerated positions near the interstitial.<sup>12</sup> In this approximation the ratio of the decay rate for a pairs to that for b pairs should be the ratio of the positions to which the vacancy can jump in the two cases, i.e., 3 to 1. This is about the same as the observed ratio of the time constants of the two exponential decays. The data indicate that defects which decay by the slower process are about twice as numerous as those decaying by the faster process. This would require that about twice as many b pairs as a pairs be formed during the irradiation. This is not unreasonable, since for every a position there are three b positions. Thus, if the energy required to displace an atom to a b position is not much greater than that required to displace it to an a position, more b pairs than a pairs could be formed during an irradiation at an electron energy which is well above threshold. The requirement on the relative displacement energies for a and b pairs is not unreasonable so that the model described above seems capable of qualitative agreement with the data.

<sup>12</sup> The movement of the vacancy toward the interstitial rather than away from it must be due to the presence of the interstitial and would seem to indicate that there should be some difference between the jump rates for vacancies in the two different pairs. The small temperature dependence of  $K_1/K_2$  is probably due to this effect.

### 7. Mobility Recovery

It was shown in Ref. 4 that the reciprocal of the Hall mobility varied linearly with the electron concentration during irradiation but that the mobility recovered faster than the carrier concentration during stage-II annealing. It can be shown that the mobility recovery is consistent with the annihilation of two different defect configurations if it is assumed that the two configurations have different scattering cross sections for the electrons. Figure 7 shows the data for the variation of reciprocal mobility with  $\varphi$  during the isothermal annealing of sample N29. The solid line was calculated by assuming that

$$\Delta(\mu_H^{-1}) = \beta_1\varphi_1 + \beta_2\varphi_2,$$

i.e., that if each substage could be observed separately, the recovery of reciprocal mobility would be linear with the carrier-concentration recovery for that substage.  $\varphi_1$  and  $\varphi_2$  were determined from the values used in making the fit to the carrier-concentration recovery data shown in Fig. 5. The ratio  $\beta_1/\beta_2$  indicates the relative scattering cross sections for the two defects. A value of 1.20 was used in fitting the data in Fig. 7. For the defect model described above, this requires that the  $a$  pairs scatter more than the  $b$  pairs. This may be associated with the fact that for  $a$  pairs the nearest neighbors of the interstitial indium atom are antimony atoms, while for  $b$  pairs they are indium atoms.

### IV. SUMMARY

A large variation in the recovery temperature, activation energy for recovery, and apparent recovery kinetics has been observed for stage-II recovery in electron-irradiated InSb. These variations can be satisfactorily accounted for by assuming that both the acceptor levels introduced into the forbidden energy band by the defects must be empty in order for the annihilation of these defects to occur. The recovery can be divided into

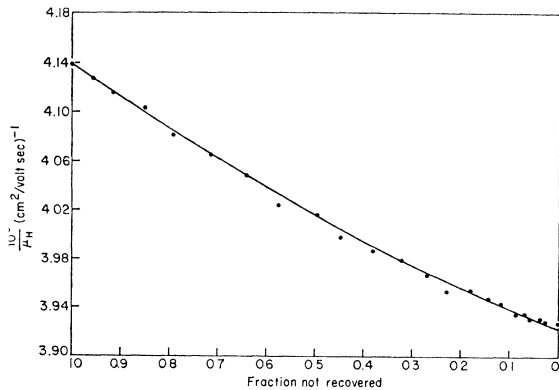


FIG. 7. Inverse Hall mobility versus fraction of damage not recovered for sample N29 during isothermal annealing following irradiation with 1.0-MeV electrons. The curve was fitted to the data points as described in the text.

two first-order processes in samples in which most of the defects have their acceptor states empty. This can be explained by assuming that two different interstitial-vacancy configurations, due to the displacement of indium atoms, are produced during the irradiation. Specific configurations and modes of annihilation of the defects during annealing are suggested that are capable of qualitative agreement with the experiments. The mobility recovery is also consistent with the production and annihilation of two different defect pairs.

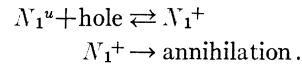
### ACKNOWLEDGMENT

It is a pleasure to acknowledge the assistance of D. R. Warner with the experiments.

### APPENDIX: RECOVERY KINETICS, TEMPERATURE, AND ACTIVATION ENERGY

#### *p*-Type Samples

Expressions are derived here for the recovery kinetics, temperature, and activation energy as a function of the carrier concentration of the sample for a single substage. *p*-type samples are treated first so that only the occupation of the lower acceptor state need be considered. Let  $N$  be the number of defects (acceptors),  $N_1^u$  the number of un-ionized acceptors, and  $N_1^+$  the number of ionized acceptors. These reactions occur:



The decay rate of the acceptors is given by

$$dN/dt = -\nu \exp(-E_m/kT) N_1^+, \quad (1)$$

where  $\nu$  is the frequency factor for the recovery process and  $E_m$  the energy of motion of the mobile defect. Assuming that the redistribution of the carriers is rapid compared to the rate of disappearance of the acceptors,

$$(N - N_1^+)p/N_1^+ = N_v \lambda_1^{-1} \exp(-E_{a1}/kT) \equiv B_1, \quad (2)$$

where  $p$  is the hole concentration,  $N_v = 2(2\pi kT m_p/h^2)^{3/2}$  is the effective density of states in the valence band,  $m_p$  is the effective mass of holes,  $E_{a1}$  is the height of the lower acceptor level above the valence-band edge, and  $\lambda_1$  is the statistical weight ratio for level 1. The hole concentration is given by

$$p = p_f + N_1^u = p_f + N - N_1^+, \quad (3)$$

where  $p_f$  is the hole concentration after the completion of recovery in the stage considered.<sup>13</sup>

On combining Eqs. (1)–(3),

$$dN/dt = -\frac{1}{2}\nu \exp(-E_m/kT) \{ p_f + 2N + B_1 \\ - [(p_f + 2N + B_1)^2 - 4N(p_f + N)]^{1/2} \}. \quad (4)$$

<sup>13</sup> This assumes that the chemical acceptors are exhausted and that the concentration of other radiation induced levels near  $E_{a1}$  is small relative to the concentration of the stage-II level at  $E_{a1}$ .

The solution to this equation may be written as

$$\left\{ \ln(X^2 - 2B_1X - p_f^2 + B_1^2) + (B_1/p_f) \ln[(X - B_1 - p_f)/(X - B_1 + p_f)] \right\} \Big|_{X(N_0)}^{X(N)} = -\nu \exp(-E_m/kT)t, \quad (5)$$

where  $X = [4B_1N + B_1(2p_f + B_1) + p_f^2]^{1/2}$ .

If  $N_1^u \ll N$ , this reduces to

$$\ln(N/N_0) = -\nu \exp(-E_m/kT)t, \quad (6)$$

i.e., when the Fermi level is well below the defect level, we have exactly first-order kinetics ( $N_0$  is the initial defect concentration). If  $N_1^+ \ll N$ , Eq. (5) reduces to

$$\ln \left[ \frac{N(N_0 + p_f)/N_0(N + p_f)}{N_0} \right] = -(p_f \lambda_1 \nu / N_0) \exp[-(E_m - E_{a1})/kT]t. \quad (7)$$

If  $N_0$  is small compared to  $p_f$ , this can be written as

$$\ln \varphi - (\Delta p/p_f)(\varphi - 1) = -(p_f \lambda_1 \nu / N_0) \times \exp[-(E_m - E_{a1})/kT]t, \quad (8)$$

where  $\varphi = N/N_0$  and  $\Delta p$  is the total change in the hole concentration for the recovery stage. This is the same form for the kinetics as in an  $n$ -type sample where only the occupation of the lower acceptor level need be considered.<sup>4</sup>

Proceeding to the recovery temperature, inspection of Eqs. (6) and (7) shows that there is an effective frequency factor which depends directly on  $p_f$  when the acceptor levels are nearly filled but which reduces to  $\nu$  when they are nearly all empty. This leads to a dependence of the recovery temperature on  $p_f$ . Specifically, we consider the temperature  $T_c$  at the center of the recovery stage on an isochronal recovery curve, which is taken as the point at which half the defects remain, i.e.,  $\varphi = 0.5$ . This may be calculated for any value of  $p_f$  if  $E_m$  and  $T_{c0}$ , the limiting value of  $T_c$  in the range of  $p_f$  where  $T_c$  no longer depends on  $p_f$ , are known. Assuming that the isochronal annealing may be approximated by a constant heating rate, i.e.,  $dT/dt = \gamma$ , Eq. (1) becomes

$$dN/N = -(\nu/\gamma) \exp(-E_m/kT)dT,$$

in the region where  $N_1^u \ll N$ . Since  $E_m/kT_{c0}$  is large, we have

$$\int_0^{T_{c0}} \exp(-E_m/kT)dT = (kT_{c0}^2/E_m) \exp(-E_m/kT_{c0})$$

as a good approximation, and

$$\ln 0.5 = (\nu kT_{c0}^2/\gamma E_m) \exp(-E_m/kT_{c0}). \quad (9)$$

A similar expression is needed for lower values of  $p_f$  in order to calculate  $T_c$  versus  $p_f$ . This is available from Eq. (7) for small enough  $p_f$ , but for intermediate values of  $p_f$ , Eq. (4) is rather cumbersome. The main effect of the change in kinetics from exact first order is noticed

for  $\varphi < 0.1$ , and this increases as  $\Delta p/p_f$  increases. This should not have an important effect on the shape of the isochronal recovery data near  $\varphi = 0.5$  so that a good approximate relation for  $dN/dT$  for the calculation of  $T_c$  can be obtained by letting  $\Delta p$  approach zero, i.e., setting  $p = p_f$  in Eq. (2). This yields

$$N_1^+ = (B_1/p_f + 1)^{-1}$$

and

$$dN/N = [\nu/\gamma(B_1/p_f + 1)] \exp(-E_m/kT)dT. \quad (10)$$

Integration of the right side of this equation is more difficult since  $B_1$  is a function of  $T$ . The main temperature dependence, however, is in the exponential in the numerator. It, therefore, seems a reasonable approximation to take the denominator outside the integral, which gives

$$\ln 0.5 = -\frac{\nu}{\gamma} \frac{1}{B_1/p_f + 1} \frac{kT_c^2}{E_m} \exp(-E_m/kT_c). \quad (11)$$

Combining Eqs. (9) and (11), we obtain

$$T_c = \frac{E_m/k}{E_m/kT_{c0} + 2 \ln(T_c/T_{c0}) - \ln(B_1/p_f + 1)}, \quad (12)$$

from which  $T_c$  is readily obtained by successive approximations since the effect of changes in the  $\ln T_c$  term and the  $\ln(B_1/p_f + 1)$  term in the denominator is small. Several comments can be made on the validity of this relation in view of approximation made in obtaining Eq. (11). When  $B_1/p_f \gg 1$  it is possible to obtain the more exact solution,

$$\ln 0.5 = -\frac{\nu}{\gamma} \frac{p_f}{B_1} \frac{kT_c^2}{E_m - E_{a1}} \exp(-E_m/kT_c).$$

The use of this result to obtain an expression for  $T_c$  would yield a change in  $T_c$  of about 0.3%, in the range of its validity. Numerical integration of Eq. (11) for  $B_1 \approx p_f$  gave a value of  $T_c$  differing by 0.1% from that calculated from Eq. (12).

The activation energy is determined from the relation

$$\ln \Delta \tau_i = C' - E/kT_i,$$

where the  $\Delta \tau_i$  are proportional to  $N^{-1}dN/dt$  at temperature  $T_i$ .<sup>9</sup> If the temperature dependence of the rate of recovery is not contained solely in a term of the form  $\exp(-E/kT)$ , the above relation will yield an effective activation energy which results from representing this temperature dependence in this form over the temperature range of the measurements. The appropriate expression to use in calculating this effective activation energy is

$$E = -k \partial \ln[N^{-1}dN/dt] / \partial (1/T). \quad (13)$$

Inserting  $dN/dt$  from Eq. (10), we obtain

$$E = E_m - (E_{a1} + \frac{3}{2}kT_c) / (1 + p_f/B_1). \quad (14)$$

### *n*-Type Samples

In *n*-type samples the possible effects of the ionization of the upper acceptor level must also be considered. If the electron concentration is sufficiently low, these acceptors are almost completely empty and the solution to the rate equation is that given in Ref. 4:

$$\ln \varphi - (\Delta n/n_f)(\varphi - 1) = -\lambda_1 N_c n_f^{-1\nu} \times \exp[-(E_m + E_g - E_{a1})/kT]t, \quad (15)$$

where the definitions of  $\Delta n$ ,  $n_f$ , and  $N_c$  are similar to those of  $\Delta p$ ,  $p_f$ , and  $\lambda_v$ , respectively, and  $E_g$  is the width of the band gap. From Eq. (15) it is seen that for

$$\Delta n \ll n_f$$

$$\frac{dN}{dT} = -\frac{\nu \lambda_1 N_c}{\gamma n_f} \exp[-(E_m + E_g - E_{a1})/kT]N. \quad (16)$$

To take account of the temperature dependence of  $E_g$ , it is assumed that  $E_g = E_{g0} - \beta T$  and that  $E_{a1}$  is independent of temperature. Integrating Eq. (16), we have, assuming only the temperature dependence of the exponential need be included in the integral as was done for Eq. (11),

$$\ln 0.5 = -\frac{\nu \lambda_1 N_c}{\gamma n_f} e^{\beta/K} \frac{kT_c^2}{E_m + E_{g0} - E_{a1}} \times \exp[-(E_m + E_{g0} - E_{a1})/kT_{c0}].$$

Combining this with Eq. (8), the result for  $T_c$  is

$$T_c = \frac{(E_m + E_{g0} - E_{a1})/k}{E_m/kT_{c0} + \ln[(T_c/T_{c0})^2 E_m / (E_m + E_{g0} - E_{a1})] + \ln(\lambda_1 N_c / n_f) + \beta/K}. \quad (17)$$

The value of the effective activation energy obtained by applying Eq. (13) in this case is

$$E = E_m + E_{g0} - E_{a1} + \frac{3}{2}kT. \quad (18)$$

In samples of increasingly higher electron concentration, the upper acceptor level will gradually become filled, and the effect of this upon the probability of annihilation of the defects must be considered. The two levels may either be independent or be successive states of ionization of a single defect. In the latter case, the upper level must be empty before the lower one can be empty. These two possibilities lead to the same equation for the rate of decay of the damage as is shown below. Quantities with a subscript two apply to the upper acceptor level. If the levels are independent, then

$$N_1^u \rightleftharpoons N_1^+ + e^-,$$

$$N_2^u \rightleftharpoons N_2^+ + e^-,$$

$$dN/dt = -\nu \exp(-E_m/kT)(N_1^+ N_2^+ / N),$$

$$N_1^+ n / (N - N_1^+) = \lambda_1 N_c \exp[-(E_g - E_{a1})/kT] \equiv B_1',$$

and

$$N_2^+ n / (N - N_2^+) = \lambda_2 N_c \exp(E_{a2}/kT) \equiv B_2.$$

$E_{a2}$  is the position of the upper level measured from the conduction-band edge, and  $n$  is the electron concentration.

$$N_1^+ \ll N$$

so that,

$$N_1^+ / N = B_1' / n,$$

and

$$dN/dt = -\nu \exp(-E_m/kT)(B_1' N_2^+ / n).$$

If the levels are not independent,

$$N_2^u \rightleftharpoons N_2^+ + e^- = N_1^u + e^-,$$

since  $N_2^+ = N_1^u$  in this case.

$$N_1^u \rightleftharpoons N_1^+ + e^-,$$

$$dN/dt = -\nu \exp(-E_m/kT)N_1^+, \quad (19a)$$

$$N_2^+ n / (N - N_2^+) = B_2,$$

and

$$N_1^+ n / N_2^+ = B_1' \quad \text{since} \quad N_1^+ \ll N_2^+. \quad (19b)$$

Therefore,

$$dN/dt = -\nu \exp(-E_m/kT)(B_1' N_2^+ / n). \quad (20)$$

Since the same relation between  $N_2^+$ ,  $N$ ,  $n$ , and  $B_2$  holds in the two cases, and  $n = n_f - 2N + N_2^+$  in both cases,  $dN/dt$  is also the same in both cases. Solving for  $N_2^+$  and substituting in Eq. (20), the result is

$$\frac{dN}{dt} = -\nu \exp(-E_m/kT) \times \frac{2N - n_f - B_2 + [(n_f + B_2 - 2N)^2 + 4B_2 N]^{1/2}}{n_f - 2N - B_2 + [(n_f + B_2 - 2N)^2 + 4B_2 N]^{1/2}} B_1'. \quad (21)$$

The solution to this equation may be written as

$$\left[ \frac{B_2}{4} \ln 2(u + B_2) + \frac{n_f(B_2 + n_f)}{B_2} \ln 2\left(\frac{u + B_2}{u}\right) - \frac{2n_f^2 + B_2 n_f}{2(u + B_2)} - \frac{B_2^3 + 4B_2 n_f(B_2 + n_f)}{8(u + B_2)^2} \right] u(N) \Big|_{u(N_0)} = \nu \exp(-E_m/kT) B_1' t, \quad (22)$$

where

$$u(N) = 2N - n_f - B_2 + [(n_f + B_2 - 2N)^2 + 4B_2N]^{1/2}.$$

This result is only valid in nondegenerate  $n$ -type samples because Eqs. (19a) and (19b) are only valid in absence of degeneracy. These may be written in the more general form

$$N_2^+/(N - N_2^+) = \lambda_2 \exp(E_F/kT) \exp(E_{a2}/kT) \\ \equiv \lambda_2 A \exp(E_{a2}/kT) \equiv A_2, \quad (23a)$$

and

$$N_1^+/N_2^+ = \lambda_1 A \exp[-(E_g - E_{a1})/kT] \equiv A_1, \quad (23b)$$

where  $E_F$  gives the position of the Fermi level measured from the conduction-band edge. In degenerate  $n$ -type samples  $N_2^+ \ll N$ , and

$$dN/dt = -\nu \exp(-E_m/kT) \lambda_1 \lambda_2 \\ \times \exp[-(E_g - E_{a1} - E_{a2})/kT] A^2 N. \quad (24)$$

The kinetics may be obtained from Eq. (24) by numerical integration, using tabulated values of  $A$ .

It is convenient to work from Eqs. (23) in deriving expressions for  $T_c$  and  $E$ , since these expressions will be valid for all  $n$ -type samples. If the approximation  $N_2^+ \ll N$  is not made, Eq. (24) then takes the form

$$dN/dt = -[A_1 A_2 / (1 + A_2)] \nu \exp(-E_m/kT) N. \quad (25)$$

If the same kind of approximation is made in integrating the equation for  $dN/dt$  as was made for  $p$ -type samples, we obtain

$$\ln 0.5 = \frac{\nu \lambda_1 \lambda_2 A^2}{\gamma(1 + A_2)} e^{\beta/K} \frac{kT_c^2}{(E_m + E_{g0} - E_{a1} - E_{a2})} \\ \times \exp[-(E_m + E_{g0} - E_{a1} - E_{a2})/kT]. \quad (26)$$

Combining this with Eq. (9), the formula for  $T_c$  is

$$T_c = \frac{(E_m + E_{g0} - E_{a1} - E_{a2})/k}{E_m/kT_{c0} + \ln[(T_c/T_{c0})^2 E_m / (E_m + E_{g0} - E_{a1} - E_{a2})] + \beta/K - 2E_F/kT + \ln[\lambda_1 \lambda_2 / (1 + A_2)]}. \quad (27)$$

Applying Eq. (13) to Eq. (25), the result for the activation energy is given by

$$E = E_m + E_{g0} - E_{a1} - E_{a2} + (2\epsilon + \epsilon A_2 - 2A_2 E_{a2}) / 2(1 + A_2), \quad (28)$$

where  $\epsilon = 2k\theta \ln A / \partial(1/T)$ . It can be shown that at low enough electron concentrations Eqs. (27) and (28) reduce to Eqs. (17) and (18), respectively.

The equation used in calculating the values of  $T_c$  for degenerate samples in Fig. 2 under the assumption that the occupation of level 2 does not affect the recovery can easily be obtained from the foregoing work. In this case,

$$dN/dt = -A_1 \nu \exp(-E_m/kT) N,$$

and

$$T_c = \frac{(E_m + E_{g0} - E_{a1})/k}{E_m/kT_{c0} + \ln[(T_c/T_{c0})^2 E_m / (E_m + E_{g0} - E_{a1})] + \beta/k - \lambda_1 E_F/kT}. \quad (29)$$